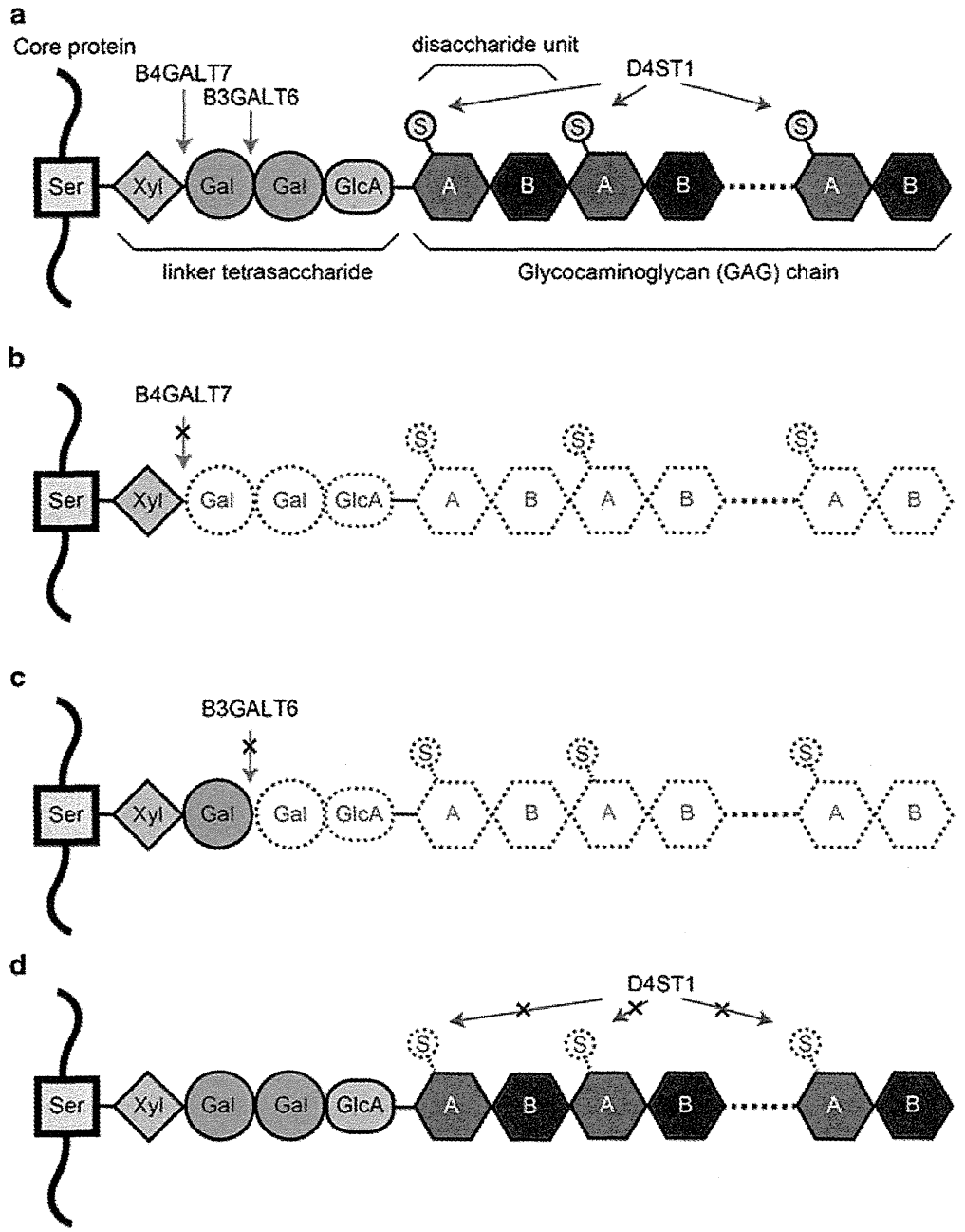

Fig. 10.1 Proteoglycan biosynthesis and its defects in two types of EDS. (**a**) Normal state. The serine residue (Ser) of the core protein and the GAG chain are bound via a linker tetrasaccharide. In CS, the disaccharides are composed of N-acetylgalactosamine (GalNAc) [position A] and glucuronic acid [position B]. In DS, the disaccharides are composed of GalNAc [position A] and Iduronic acid (IdoA) [position B]. B4GALT7 and B3GALT6 add the first and second galactose (Gal) to the xylose of the linker tetrasaccharide (*green arrows*). D4ST1 then adds the active sulfate to the 4-*O* position of GalNAc (*red arrows*) on DS. (**b**, **c**) Progeroid type of EDS. The impaired B4GALT7 cannot elongate the glycan chain from the first galactose (**b**). The impaired B3GALT6 cannot add the second galactose and the following glycan chain (**c**). (**d**) D4ST1-deficient EDS. The impaired/inactive D4ST1 cannot add the sulfate to GalNAc. *Gal* galactose, *GlcA* glucuronic acid, *S* active sulfate, *Ser* serine, *Xyl* xylose

residue of the core protein, GalNAc (*N*-acetyl galactosamine) transferase I elongates the glycan branch to create CS/DS. The enzyme C5-carboxy epimerase transforms glucuronic acid (GlcA) to iduronic acid (IdoA), which is specific for dermatan/DS (Fig. 10.3a). DS actually exists in a CS/DS hybrid state, containing GlcA–GalNAc and IdoA–GalNAc disaccharides (Figs. 10.2b

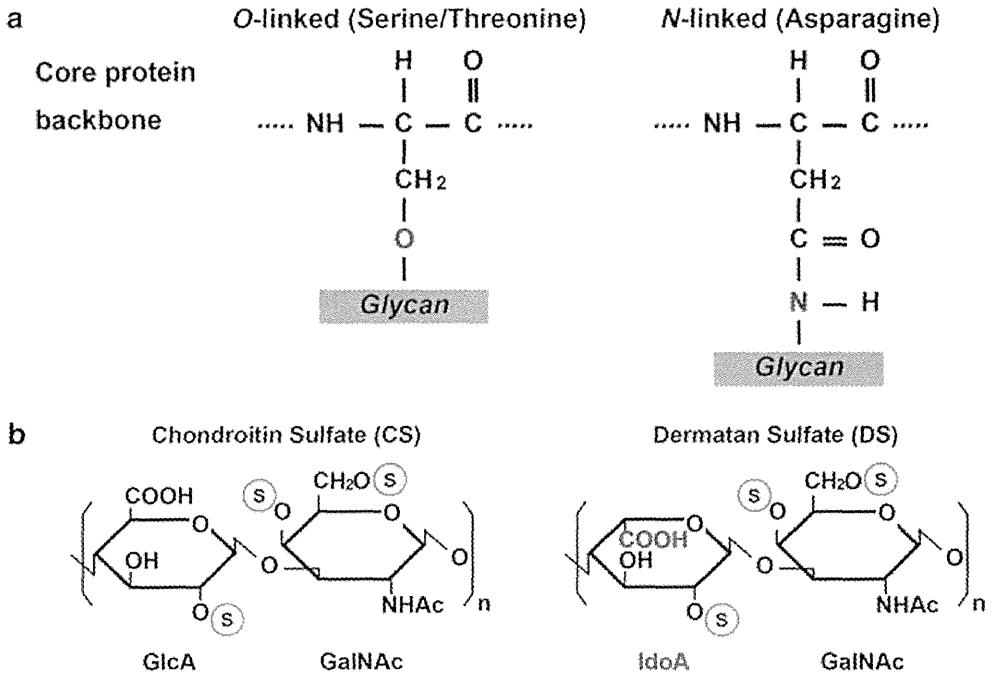

Fig. 10.2 Chemical structures of proteoglycan and disaccharides. (**a**) Chemical structure of *O*-linked and *N*-linked glycan. *O*-linked glycan can be linked via the *O*-element of serine or threonine. The diagram shows linking for serine. (**b**) Chemical structures of the disaccharide units of CS (*left*) and DS (*right*)

and 10.3a) [12]. Dermatan 4-*O*-sulfotransferase 1(D4ST1) specifically transfers an active sulfate to the 4-*O* position on the GalNAc residue of dermatan. The transfer of the active sulfate is impaired in D4ST1-deficient EDS (Figs. 10.1d and 10.3b).

10.3 The Progeroid Type of EDS (type 1: MIM#130070, type2: MIM#615349)

Alternative Names (MIM#130070)
Xylosylprotein 4-β-galactosyltransferase deficiency
XGPT deficiency
Galactosyltransferase I deficiency

10.3.1 Clinical Manifestations

Hernandez et al. reported five unrelated males in 1979, 1981, and 1986 representing a distinct variant of EDS. These males presented with a progeroid facial appearance, mild intellectual disability, and multiple nevi, in addition to hyperextensibility and fragility of skin, a high propensity for bruising, and joint hypermobility (particularly of the digits) [16–18]. A wrinkled face, curly and fine hair, scant eyebrows/eyelashes, telecanthus, periodontitis, multiple caries, low set/prominent ears, pectus excavatum, winged scapulae, and pes planus were observed in all five patients. Cryptorchidism and inguinal hernia were also noticed in four of the patients. Interestingly, the occurrence of the disorder in all of these patients was sporadic and the ages of their fathers were relatively advanced (33–55 years old). These characteristics prompted Hernandez et al. to speculate that the syndrome is caused by a de novo mutation [16].

In 1987, Kresse et al. reported a Danish male patient who was born to non-consanguineous healthy parents [26]. This patient presented with the clinical features observed in the original five patients, as well as a triangular head with a tiny face, frontal bossing, mid-face hypoplasia, a broad nasal bridge, prominent deep-set eyes, a small mouth, dental anomalies, low-set ears,

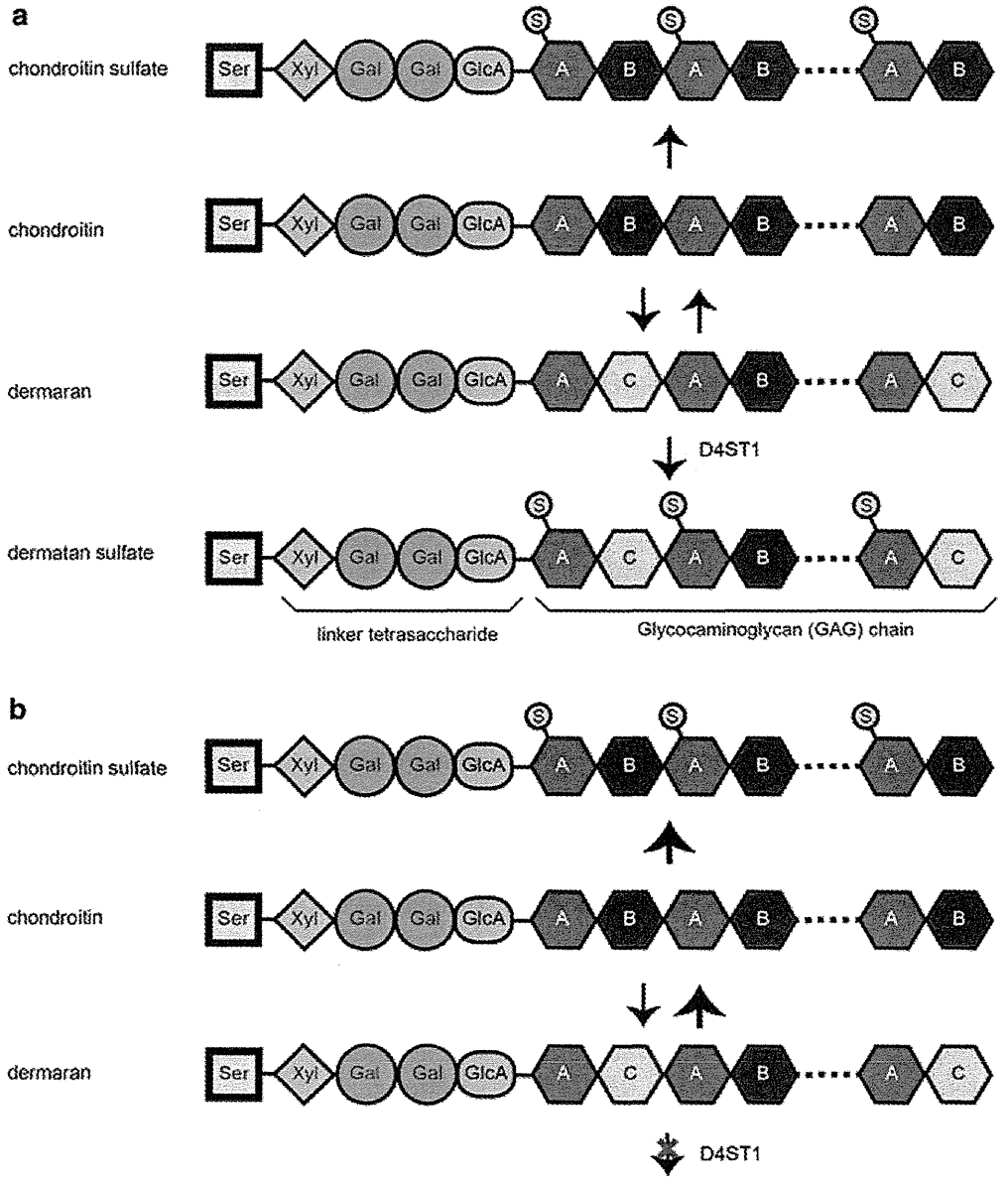

Fig. 10.3 Effects of D4ST1 defects on the biosynthesis of CS and DS. (**a**) The starting structure is chondroitin with a repeating disaccharide consisting of GalNAc [position A] and GlcA [position B]. Sulfation by 6-*O*-GalNAc sulfotransferase and 4-*O*-GalNAc sulfotransferase creates CS from chondroitin. To produce DS, first, C5-carboxy epimerase replaces GlcA with IdoA [position C]. This process is bidirectional as indicated by the bi-directional arrows. Then, D4ST1 adds sulfates to dermatan creating DS and prevents back epimerization. DS is often detected as a CS/DS hybrid. (**b**) In D4ST1-deficient EDS, back epimerization from IdoA to GlcA occurs. Consequently, neither DS nor dermatan are detected in fibroblasts derived from patients. *Gal galactose*, *GlcA* glucuronic acid, *S* active sulfate, *Ser* serine, *Xyl* xylose

short stature, osteopenia of all bones, dysplasia of some bones, and hypotonia. In 2004, Faiyaz-Ul-Haque et al. reported two patients from a large consanguineous Qatari family. The clinical features of both Qatari patients and the Danish patient seemed to be different from those of the original five patients [14].

10.3.2 Genetic Information

10.3.2.1 B4GALT7

In 1999, two different research groups [1, 33] identified compound heterozygous mutations of gene for xylosylprotein beta 1,4-galactosyltransferase, polypeptide 7 (*B4GALT7*, NM_007255.2),

c.557C>A (p.Ala186Asp) and c.617T>C (p. Leu206Pro) in the Danish patient reported by Kresse in 1987 [26]. The two Qatari patients from a large consanguineous family were analyzed in 2004 [14]. Based on the hypothesis of autosomal recessive inheritance, haplotype analysis using microsatellite markers for the limited candidate loci delineated a homozygous region from *D5S469* and *D5S2111*, which harbors *B4GALT7* [14]. A homozygous missense mutation (c.808C>T, p.Arg270Cys) in *B4GALT7* was identified. Interestingly, the clinical phenotype of the Qatari patients was milder than that of the Danish one.

B4GALT7 was cloned by Okajima et al. [34]. The gene consists of six coding exons with a 948-bp open reading frame. This gene encodes xylosylprotein β-1,4-galactosyltransferase, polypeptide 7 (B4GALT7; aliases: galactosyltransferase I, XGPT1, and XGALT1), which is 327 amino acids long and its molecular weight is 37.4 kDa. B4GALT7 is a type II transmembrane protein localized in the Golgi apparatus, and is a key initiator of GAG synthesis as it attaches the first galactose of the linker tetrasaccharide of PGs (Fig. 10.1a, b).

10.3.2.2 B3GALT6

In 2013, Nakajima et al. have identified compound heterozygous mutations of *B3GALT6* (NM_080605.3) in three patients with progeroid form of EDS [32]. This intronless gene has a 990-bp open reading frame and encodes UDP-Gal:βGal β 1,3-galactosyltransferase polypeptide 6 (alternatively galactosyltransferase -II: GalT-II), which is 329 amino acids long and its molecular weight is 37.1kDa. It is also the type II transmembrane protein localized in the Golgi apparatus, and it attaches the second galactose of the tetrasaccharide linker of PGs (Fig. 10.1a, c). So far, two missense (c.16C>T, p.Arg6Trp and c.925T>A, p.Ser309Thr), two frameshift deletions (c.353delA, p.Asp118Alafs*160 and c.588delG, p.Arg197Alafs*81) and one in-frame deletion (c.415_423del, p.Met139Ala141del) were reported in this type of EDS [32].

10.3.3 Biochemical Characteristics

10.3.3.1 B4GALT7

Kresse et al. reported that their patient's fibroblasts produced only PG chain-free core proteins (molecular weight: 46 and 44 kDa) whereas control fibroblasts produced normal PG chains [26]. Additionally, the GAG-free core protein in that patient contained unsubstituted xylose residues (Fig. 10.1b).

Okajima et al. measured the enzyme activity of exogenously expressed proteins (wild type, p. Ala186Asp, p.Leu206Pro) in XGalT-1/B4GALT7-deficient CHO cells [33]. In total cell lysates, the enzyme activity of the p.Ala186Asp mutant was approximately 50 % lower than that of the wild-type protein, whereas the activity of the p. Leu206Pro mutant was almost undetectable. Interestingly, the wild-type and p.Ala186Asp proteins were localized in the Golgi apparatus whereas the p.Leu206Pro mutant existed in the cytoplasm. The α-helix disrupted by p.Leu206Pro may alter the protein's conformation, thus impairing intracellular trafficking and enzyme activity [33].

B4GALT7 activity in fibroblasts from another patient with a homozygous mutation, c.808C>T (p. Arg270Cys), was also lower than that of controls [40]. The extracellular matrix around the $B4GALT7^{Arg270Cys}$ mutant fibroblasts was disorganized without banded fibrils. Furthermore, the proliferation of $B4GALT7^{Arg270Cys}$ fibroblasts was significantly reduced to 45 % of the level of control fibroblasts [40].

Bui et al. measured galactosyltransferase activity of B4GALT7 mutants expressed in CHO pgsB-618 cells using 4-methylumbelliferyl-β-D-xylopyranoside as acceptor substrate. The enzyme activities of the p.Arg270Cys, p. Ala186Asp, and p.Leu206Pro mutants were decreased to 60, 11, and 0 % (undetectable) of that of the wild-type enzyme [4]. It has been reported that the clinical features of patients with the homozygous p.Arg270Cys mutation appear to be milder than those of patients with compound heterozygous mutations, including p. Ala186Asp or p.Leu206Pro, supporting the different effects of these mutations.

10.3.3.2 B3GALT6

Nakajima et al. measured the galactosyltransferase activity of *B3GALT6* in vitro using soluble-FLAG-tagged proteins for wild-type and mutant (p.Ser309Thr) which was observed common in two families and revealed the enzyme activity of the mutant protein was significantly decreased compared to the wild-type [32].

10.4 D4ST1-Deficient EDS (MIM#601776)

Alternative Names
Ehlers–Danlos syndrome, type VIB, formerly
Ehlers–Danlos syndrome, Kosho type
Ehlers–Danlos syndrome, musculocontractural type
Adducted thumbs, clubfoot, and progressive joints and skin laxity syndrome
Adducted thumb-clubfoot syndrome (ATCS)
Dündar syndrome
Arthrogryposis, distal, with peculiar faces and hydronephrosis

10.4.1 Clinical Manifestations

The kyphoscoliosis type of EDS (formerly known as, EDS type VI) is characterized by generalized joint laxity, severe muscular hypotonia and scoliosis at birth, scleral fragility, and rupture of the ocular globe [2]. This disorder is essentially caused by lysyl hydroxylase deficiency (EDS type VIA); other patients with similar clinical manifestations but without lysyl hydroxylase deficiency were classified as EDS type VIB.

In 2005, Kosho et al. reported two unrelated patients with fragile and hyperextensible skin, a high propensity for bruising, generalized joint laxity, kyphoscoliosis, and the major features of EDS VI, as well as a characteristic craniofacial appearance, and multiple congenital contractures [25]. Lysyl hydroxylase deficiency was excluded in these patients by analysis of the urinary deoxypyridinoline:pyridinoline ratio, and the patients were tentatively classified as EDS VIB. Kosho et al. subsequently reported on four additional unrelated patients and concluded that the patients represented a new type of EDS [23]. Notably, all six patients had homozygous or compound heterozygous mutations in *CHST14* [31]. Loss-of-function mutations in *CHST14* were independently found in 11 patients from four families with a rare arthrogryposis syndrome known as "adducted thumb-clubfoot syndrome (ATCS)" [9–11, 21, 43] and in three patients from two families who were originally classified as suffering from EDS VIB [27]. Malfait et al. suggested that these patients had the same disorder, which they termed "musculocontractural EDS" [27]. Shimizu et al. described the clinical characteristics of two additional patients together with a review of all of the patients reported at that time; their findings support the notion that the three independently identified conditions represent a single type of EDS [41]. Conversely, Janecke et al. claimed that the disorder should not be categorized as a type of EDS because of the presence of atypical clinical features, including facial dysmorphism, multiple congenital contractures, visceral anomalies, and impaired biosynthesis of DS as a cause of the disorder, and proposed the term DS-deficient adducted thumb-clubfoot syndrome [20]. In their response, Kosho et al. provided clinical and etiological evidence from which the disorder could be categorized as a type of EDS, because of the presence of all major features of EDS, including connective tissue fragility which required special and appropriate management of these patients. Decorin-mediated impaired assembly of collagen fibrils was the primary cause of progressive connective tissue fragility in this type [24]. Therefore, Kosho et al. proposed that the term D4ST1-deficient EDS (adducted thumb-clubfoot syndrome) was appropriate for this syndrome [24]. The current OMIM (http://www.ncbi.nlm.nih.gov/omim) registration of this disorder is EDS, musculocontractural type.

To date, descriptions of 26 patients (12 males, 14 females) from 17 families have been published [9–11, 21, 23, 25, 27, 30, 31, 41, 43, 46,

Table 10.1 Classification of Ehlers-Danlos syndrome

	Prevalence/patient number	Inheritance	Causative gene
Major types			
Classical type	1/20,000	AD	*COL5A1*, *COL5A2*
Hypermobility type	1/5,000–20,000	AD	Unknown[a]
Vascular type	1/50,000–250,000	AD	*COL3A1*
Kyphoscoliosis type	1/100,000	AR	*PLOD1*
Arthrochalasia type	30	AD	*COL1A1*, *COL1A2*
Dermatosparaxis type	8	AR	*ADAMTS2*
Other types			
Brittle cornea syndrome	11	AR	*ZNF469*
EDS-like syndrome due to tenascin-XB deficiency	10	AR	*TNXB*
Progeroid form	7	AR	*B4GALT7*, *B3GALT6*
Cardiac valvular form	4	AR	*COL1A2*
EDS-like spondylocheirodysplasia	8	AR	*SLC39A13*
D4ST1-deficient EDS (DD-EDS)	22	AR	*CHST14*

AD, autosomal dominant; *AR*, autosomal recessive; *COL5A1*, collagen, type V, alpha 1; *COL5A2*, collagen, type V, alpha 2; *COL3A1*, collagen, type III, alpha 1; *PLOD1*, procollagen-lysine, 2-oxoglutarate 5-dioxygenase 1; *COL1A1*, collagen, type I, alpha 1; *COL1A2*, collagen, type I, alpha 2; *ADAMTS2*, ADAM metallopeptidase with thrombospondin type 1 motif, 2; *ZNF469*, zinc finger protein 469; *TNXB*, tenascin XB; *B4GALT7*, xylosylprotein beta 1,4-galactosyltransferase, polypeptide 7; *B3GALT6*, UDP-Gal:βGal β 1,3-galactosyltransferase polypeptide 6; *COL1A2*, collagen, type I, alpha 2; *SLC39A13*, solute carrier family 39 (zinc transporter), member 13; *CHST14*, carbohydrate (*N*-acetylgalactosamine 4-*0*) sulfotransferase 14

[a] *TNXB* mutations in a small subset of patients

48, 49]. This syndrome is characterized by a unique set of clinical features consisting of progressive systemic manifestations, including tissue fragility (e.g., skin hyperextensibility and fragility, progressive spinal and foot deformities, and large subcutaneous hematomas) and various malformations (e.g., facial features, congenital eye/heart/gastrointestinal defects, congenital multiple contractures). We have summarized the main clinical features of this syndrome in each organ in Table 10.1

10.4.1.1 Craniofacial Features

The characteristic craniofacial features apparent at birth or during early infancy include a large fontanelle, hypertelorism, short and down slanting palpebral fissures, blue sclerae, a short nose with hypoplastic columella, low-set and rotated ears, a high or cleft palate, a long philtrum, a thin upper-lip vermilion, a small mouth, and micro-retrognathia (Fig. 10.4a, b). Slender and asymmetrical facial shapes with a protruding jaw are generally observed from school age onwards (Fig. 10.4c, d).

10.4.1.2 Skeletal Features

Congenital multiple contractures, particularly adduction-flexion contractures of the thumbs and talipes equinovarus, are the main skeletal features (Fig. 10.4e, g, h). Fingers with a "tapering", "slender", and "cylindrical" shape are also common (Fig. 10.4f). Aberrant finger movement was described in three patients. Four patients had tendon abnormalities, including anomalous insertion of the flexor muscles, which probably caused the congenital contractures. Spinal deformities (e.g., scoliosis and kyphoscoliosis) and talipes deformities (e.g., planus and valgus) (Fig. 10.4i) occurred and progressed during childhood. Marfanoid habitus, recurrent joint dislocations, and pectus deformities (e.g., flat and thin, excavatum, and carinatum) were also evident. Bone mineral density was decreased in five patients and normal in two. Urine concentrations of the N-telopeptide of collagen type I, an osteoclast marker, were increased in three patients, whereas serum bone-specific alkaline phosphatase concentrations, an osteoblast marker, were normal in three, suggesting that

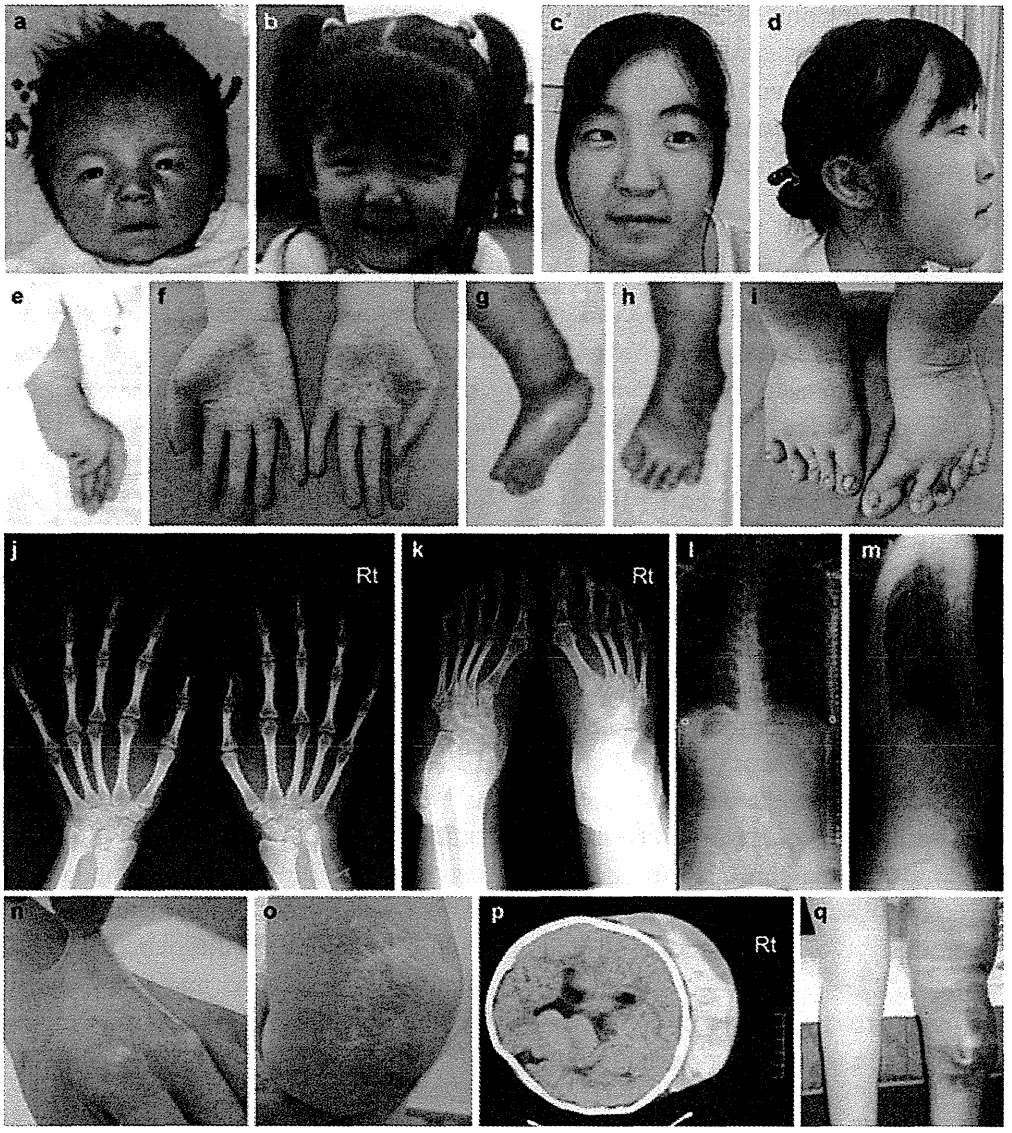

Fig. 10.4 Clinical photographs of patients with D4ST1-deficient EDS. (**a–d**) Facial features of a patient at 23 days (**a**), 3 years (**b**), and 16 years (**c**, **d**) of age. (**e**, **f**) Images of the hand in a patient with an adducted thumb at 1 month of age (**e**) and cylindrical fingers at 19 years of age (**f**). (**g–i**) Images of the foot in a patient with bilateral clubfeet at 1 month of age (**g**, **h**) and progressive talipes deformities (planus and valgus) at 19 years of age (**i**). (**j–m**) Radiographs of a 16-year-old patient show diaphyseal narrowing of the phalanges and metacarpals (**j**, **k**) and kyphoscoliosis with tall vertebral bodies (**l**, **m**). (**n**, **o**) Cutaneous features of a 19-year-old patient with hyperextensibility (**n**), atrophic scars, and fistula formation (**o**). (**p**) A massive cranial subcutaneous hematoma in the head of a 6-year-old patient after falling onto the floor. (**q**) A subcutaneous hematoma in the leg of a 16-year-old patient (All figures were originally published in Kosho et al. [23] except Fig. 10.4p, which was published in Kosho et al. [25])

increased osteoclast activity but normal osteoblast activity could cause osteopenia or osteoporosis. Radiologically, diaphyseal narrowing of the phalanges and metacarpals was noted in six patients (Fig. 10.4j, k). Talipes valgus and planus or cavum, with diaphyseal narrowing of the phalanges and metatarsals, were noted in six patients. Tall vertebral bodies were noted in five patients (Fig. 10.4l, m).

10.4.1.3 Cutaneous Features

Cutaneous features were apparent in most patients, including hyperextensibility to redundancy (Fig. 10.4n), a high propensity for bruising,

fragility leading to atrophic scars (Fig. 10.4o), acrogeria-like fine palmar creases or wrinkles, hyperalgesia to pressure, and recurrent subcutaneous infections with fistula formation. The palmar creases increased and became deeper with age.

10.4.1.4 Cardiovascular Features

Large subcutaneous hematomas were common, and frequently required intensive treatment, including hospital admission, blood transfusion, and surgical drainage (Fig. 10.4p, q). The lesions were thought to be caused by the rupture of a subcutaneous artery or vein. Bleeding time was prolonged in two patients (9 min and 11 min) and was normal in three. Intranasal administration of 1-desamino-8-D-arginine vasopressin prevented the development of large subcutaneous hematomas after trauma [49]. Four patients had congenital heart defects including an atrial septal defect in three, a patent ductus arteriosus in one, and coarctation of the aorta in one. Five patients had cardiac valve abnormalities including one who underwent surgery for infectious endocarditis, which was probably caused by aortic valve or mitral valve regurgitation.

10.4.1.5 Respiratory Features

Three adult patients developed pneumothorax or hemopneumothorax requiring chest tube drainage.

10.4.1.6 Gastrointestinal Features

Numerous gastrointestinal abnormalities were reported, including diverticular perforation in two adult patients, constipation in seven patients, abdominal pain in two patients, and other disorders in one patient (common mesentery, absence of the gastrocolic omentum with a spontaneous volvulus of small intestine, gastric ulcer, and malrotation with duodenal obstruction).

10.4.1.7 Genitourinary Features

Urological complications included nephrolithiasis or cystolithiasis in five patients, hydronephrosis in three, a dilated or atonic bladder with recurrent urinary tract infection in two, and a horseshoe kidney in one. Cryptorchidism was observed in eight male patients, including one who underwent orchiopexy because of hypogonadism in adulthood. Poor breast development was noted in five adolescent or adult patients. No pregnant females have been reported.

10.4.1.8 Ophthalmologic Features

Various ophthalmological complications have been reported, including strabismus in 12 patients, refractive errors in nine, glaucoma or elevated intraocular pressure in six, microcornea or microphthalmia in three, and retinal detachment in three.

10.4.1.9 Hearing Impairment

Six patients had hearing impairments, including for high-pitched sounds in three.

10.4.1.10 Growth

Patients showed mild prenatal growth retardation as the mean birth length was −0.5 standard deviations (SD), the mean birth weight was −0.6 SD, and the mean birth occipitofrontal circumference (OFC) was −0.2 SD. Postnatal growth was also mildly impaired, as the patients were generally slender with relative macrocephaly. The mean height was −0.9 SD, the mean weight was −1.5 SD, and the mean OFC was −0.2 SD.

10.4.1.11 Development and Neuromuscular Features

Gross motor developmental delay was observed in 14 patients, as the median age of independent walking was 2 years 1 month. Two patients, aged 15 years and 32 years, could not walk unassisted. An underlying myopathic process was observed in two patients. Mild intellectual disability was apparent in four patients. One patient had a global psychomotor delay at 1.5 years of age, but his intellectual quotient was approximately 90 at the age of 7 years 2 months. Brain imaging showed ventricular enlargement and/or asymmetry in seven patients, absence of the left septum pellucidum in one patient, and a short corpus callosum, mildly prominent Sylvian fissures, and periventricular nodular heterotopias. Two patients had spinal cord tethering.

10.4.2 Genetic Information

Autosomal recessive inheritance was considered based on the presence of this syndrome in consanguineous families [11, 27, 31]. Three independent groups have performed homozygosity mapping and/or linkage analysis and each showed that the gene carbohydrate (*N*-acetylgalactosamine 4-*O*) sulfotransferase 14 (*CHST14*, NM_130468.3) was responsible for this syndrome [11, 27, 31].

The *CHST14* gene was first cloned by Evers et al. [13]. It contains one coding exon (1,131-bp open reading frame) and is localized at 15q15.1. This gene encodes D4ST1, a 376 amino acid type II transmembrane protein (molecular weight: 43 kDa), that is localized in the Golgi membrane. It transfers a sulfate group from 3′-phosphoadenosine 5′-phosphosulfate to position 4 of the GalNAc residues in dermatan to generate DS (Figs. 10.1a and 10.3a). Northern blotting revealed that *CHST14* is mainly expressed in heart, placenta, liver, and pancreas, and is weakly expressed in lung, skeletal muscle, and kidney [13].

To date, 11 pathogenic mutations of *CHST14* have been identified: p.Val49*, p.Lys69*, p.Arg135_Leu137delinsGlyThrGln, p.Phe209Ser, p.Arg213Pro, p.Lys226Alafs*16, p.Arg274Pro, p.Pro281Leu, p.Cys289Ser, p.Tyr293Cys, and p.Glu334Glyfs*107 [11, 27, 30, 31, 46, 48]. (p.Val48* was corrected to p.Val49*; Erratum in Am J Med Genet Part A 161A(2):403 (2013)) (p.Arg135Gly and p.Leu137Gln were originally reported by Dündar et al., but lately registered as c.403_410delCGCACCCTinsGGCACCCA, p.Arg135_Leu137delinsGlyThrGln in The Human Gene Mutation Database: https://portal.biobase-international.com/hgmd/pro/genesearch.php). Because these are protein truncation mutations and missense mutations, it seems likely that the mutations cause a loss of function.

10.4.3 Biochemical Information

Dündar et al. reported that DS-derived IdoA-GalNAc(4S) disaccharide was undetectable in fibroblasts derived from a patient with a homozygous p.Arg213Pro mutation. They also reported that GlcA-GalNAc(4S) content was greatly increased in the fibroblast extract and the culture media obtained from cultures of fibroblasts derived from this patient as compared with control fibroblasts [11]. It was also found that the amount of nonsulfated disaccharides (GlcA-GalNAc and IdoA-GalNAc) was increased in the cell extract and its media from the patient's fibroblast as compared with normal control fibroblasts. From these results, Dündar et al. proposed that epimerization of GlcA to IdoA by C5-carboxy epimerase is followed by sulfation of the C4 hydroxyl on the adjacent GalNAc residue by D4ST1. This process generates DS from dermatan and prevents back-epimerization from IdoA to GlcA [11, 28].

Miyake et al. measured the sulfotransferase activity of COS7 cells transfected with wild-type and mutant D4ST1 harboring the p.Lys69*, p.Pro281Leu, p.Cys289Ser, or p.Tyr293Cys mutations. The enzyme activity of the mutants was as low as that in mock transfected cells, suggesting that these missense mutations result in the loss of function [31]. The disaccharide composition of the decorin GAG chain isolated from the patient's fibroblasts consisted only of CS, without DS, while the chains isolated from normal fibroblasts consisted of CS/DS hybrid chains [31]. Furthermore, the level of nonsulfated dermatan was negligible in the patient's fibroblasts [31]. Thus, in this syndrome, the CS/DS chain is replaced with the CS chain, even though the core proteins are normal.

10.4.4 Pathology and Pathophysiology

Of the major DS proteoglycans in skin, decorin was a focus of research because it binds to collagen fibrils via its core protein and its GAG chains act as interfibrillar bridges [38, 39]. Three α collagen chains are self-assembled to generate tropocollagen, in the form of a triple helix. Tropocollagen then self-assembles to form collagen fibrils via decorin (Fig. 10.5a). Collagen fibrils are assembled into a collagen fiber, known as the collagen bundle, via the antiparallel com-

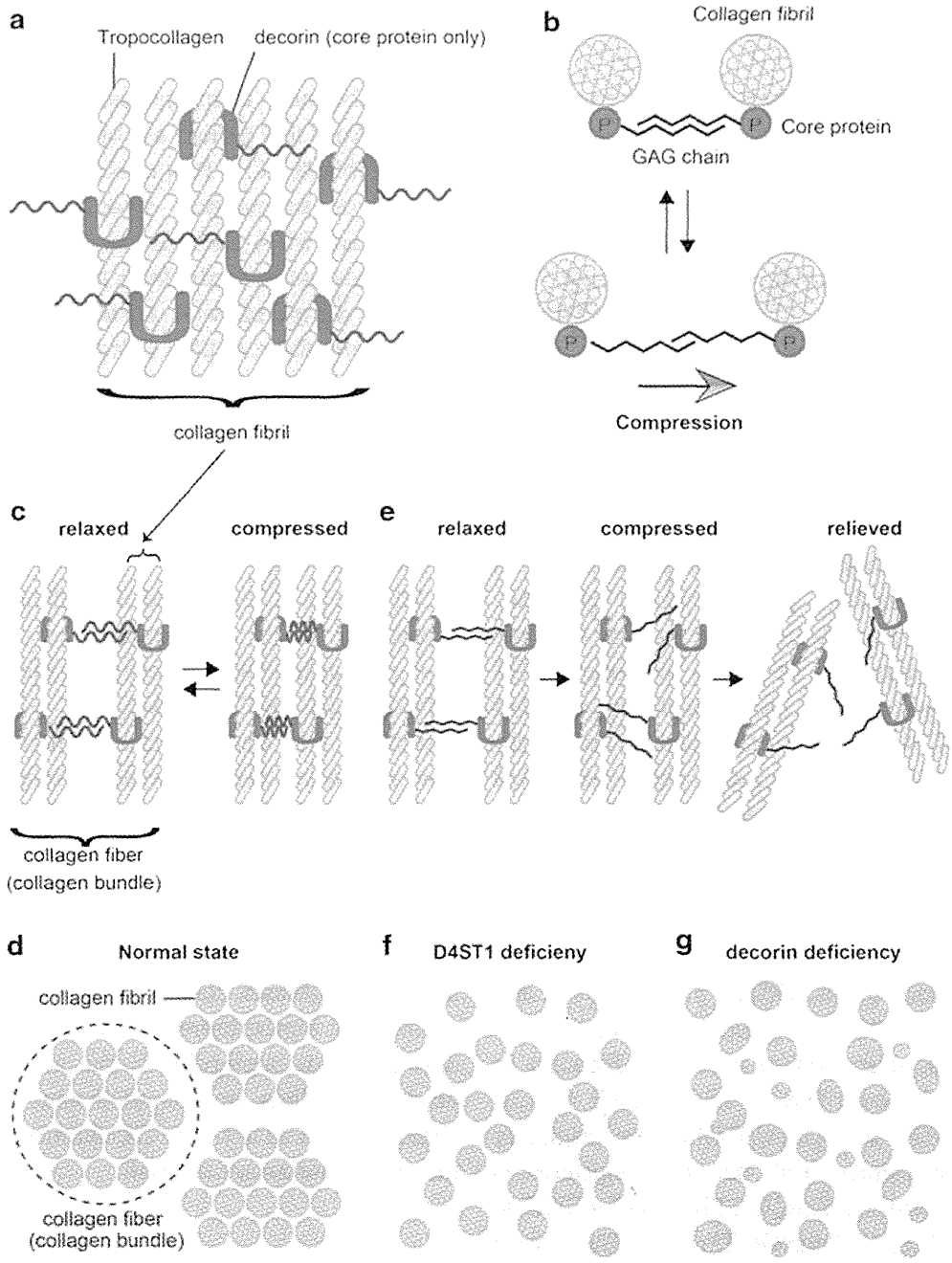

Fig. 10.5 Putative model of abnormal collagen bundle assembly in D4ST1-deficient EDS. (**a**) Tropocollagen directly binds to decorin and forms a collagen fibril. The *blue lines* represent the CS/DS hybrid chain. (**b**) Illustration of the sliding filament model showing reversible longitudinal slippage between the antiparallel GAG chains. The *black lines* represent unspecified GAGs. (**c**, **d**) In the normal state, the CS/DS chains can bend against the direction of mechanical compression and rebound to the original structure (**c**). Thus, the collagen bundles are refractory to compression stress (**d**). (**e**, **f**) In D4ST1-deficient EDS, the CS/DS chains are replaced with CS chains (*red lines*). These chains cannot resist mechanical compression, resulting in irreversible scattering of the collagen fibrils. (**g**) The size and shape of the collagen fibrils are highly variable in decorin-deficient mice

plex of the CS/DS hybrid GAG chains of decorin, which acts like a bridge to provide a space between individual fibrils and tighten the collagen fiber (Fig. 10.5c, d).

The GAGs span collagen fibrils in the extracellular matrix of skin and tendons, and the length of the GAG chain determines the width of the interfibrillar gap [35, 36]. Elasticity of the

extracellular matrix is explained by the sliding filament model, which allows reversible longitudinal slippage between the antiparallel GAG chains (Fig. 10.5b) [39]. Because tissue stability and elasticity depend on the structure of the GAG bridges, irreversible damage can occur if the bridges are inelastic [39].

Decorin is composed of a horseshoe-shaped core protein (molecular weight: ~45 kDa) and a single CS/DS hybrid chain on the N-terminal side (Fig. 10.5a) [22, 47]. Weber et al. reported that the model structure of decorin consists of an arch in which the inner concave surface is formed from a curved β-sheet and the outer convex surface is formed from α-helices. They also proposed that one tropocollagen fiber lies within the decorin convex and another interacts with one arm of the arch [47]. The IdoA:GlcA ratio in DS ranges from ~10 to >90 % depending on the tissue type [39]. Importantly, L-IdoA residues in DS can easily undergo conformational changes, unlike GlcA in CS [6, 7]. Thus, the IdoA:GlcA ratio should be higher in more flexible tissues [39].

Light microscopic investigation of skin specimens from two patients showed that fine collagen fibers were predominant in the reticular to papillary dermis and the number of thick collagen bundles was markedly reduced [31]. Electron microscopic examination of the specimens showed that collagen fibrils were dispersed throughout the reticular dermis, whereas they were regularly and tightly assembled in control tissue. Surprisingly, each collagen fibril was smooth and round, with little variation in size or shape, similar to the fibril in the control tissue (Fig. 10.5d, f) [31]. The disaccharide composition of the decorin GAG chain from a patient's fibroblasts only consisted of CS, without DS disaccharide, whereas control fibroblasts consisted of a CS/DS hybrid [31]. The transition of decorin from the CS/DS hybrid chain to a CS chain probably decreases the flexibility of the GAG chain. The sliding filament model proposes that mechanical compression might also work in the CS chain of D4ST1-deficient patients, but the inflexibility of the CS chain is unable to tolerate higher mechanical pressures or is too inelastic to maintain normal skin properties (Fig. 10.5e, f). This irreversible event could explain the progressive clinical course of this disease.

Interestingly, there were marked variations in the size and shape of dermal collagen fibrils in decorin-null mice (Fig. 10.5g) [8]. These findings suggest that the decorin core protein is important for collagen fibril formation, and that the CS/DS hybrid chain of decorin PG regulates the space between the collagen fibrils and form collagen bundles, as previously reported [37]. These findings suggest that the main pathological basis of this disorder could be insufficient assembly of collagen fibrils.

However, Dündar et al. reported that the light microscopic and electron microscopic findings of a patient's skin were unchanged compared to the normal control [11]. Malfait et al. reported that, in their patient, most collagen bundles were small diameter in size, and some were composed of collagen fibrils of varying diameter that were separated by irregular interfibrillar spaces [27]. In addition, the fibroblasts exhibited an elongated and/or dilated endoplasmic reticulum. So far, definitive histopathologic characteristics have not been established, so further studies are strongly encouraged to determine the major histological characteristics and underlying pathophysiology of this disorder.

References

1. Almeida R, Levery SB, Mandel U, Kresse H, Schwientek T, Bennett EP, Clausen H (1999) Cloning and expression of a proteoglycan UDP-galactose:beta-xylose beta1,4-galactosyltransferase I. A seventh member of the human beta4-galactosyltransferase gene family. J Biol Chem 274:26165–26171
2. Beighton P, De Paepe A, Steinmann B, Tsipouras P, Wenstrup RJ (1998) Ehlers-Danlos syndromes: revised nosology, Villefranche, 1997. Ehlers-Danlos National Foundation (USA) and Ehlers-Danlos Support Group (UK). Am J Med Genet 77:31–37
3. Bishop JR, Schuksz M, Esko JD (2007) Heparan sulphate proteoglycans fine-tune mammalian physiology. Nature 446:1030–1037
4. Bui C, Talhaoui I, Chabel M, Mulliert G, Coughtrie MW, Ouzzine M, Fournel-Gigleux S (2010) Molecular characterization of beta1,4-galactosyltransferase 7 genetic mutations linked to the progeroid form of Ehlers-Danlos syndrome (EDS). FEBS Lett 584:3962–3968
5. Bulow HE, Hobert O (2006) The molecular diversity of glycosaminoglycans shapes animal development. Ann Rev Cell Dev Biol 22:375–407
6. Casu B, Petitou M, Provasoli M, Sinay P (1988) Conformational flexibility: a new concept for explaining binding and biological properties of iduronic acid-

containing glycosaminoglycans. Trends Biochem Sci 13:221–225
7. Catlow KR, Deakin JA, Wei Z, Delehedde M, Fernig DG, Gherardi E, Gallagher JT, Pavao MS, Lyon M (2008) Interactions of hepatocyte growth factor/scatter factor with various glycosaminoglycans reveal an important interplay between the presence of iduronate and sulfate density. J Biol Chem 283:5235–5248
8. Danielson KG, Baribault H, Holmes DF, Graham H, Kadler KE, Iozzo RV (1997) Targeted disruption of decorin leads to abnormal collagen fibril morphology and skin fragility. J Cell Biol 136:729–743
9. Dündar M, Demiryilmaz F, Demiryilmaz I, Kumandas S, Erkilic K, Kendirci M, Tuncel M, Ozyazgan I, Tolmie JL (1997) An autosomal recessive adducted thumb-club foot syndrome observed in Turkish cousins. Clin Genet 51:61–64
10. Dündar M, Kurtoglu S, Elmas B, Demiryilmaz F, Candemir Z, Ozkul Y, Durak AC (2001) A case with adducted thumb and club foot syndrome. Clin Dysmorphol 10:291–293
11. Dündar M, Müller T, Zhang Q, Pan J, Steinmann B, Vodopiutz J, Gruber R, Sonoda T, Krabichler B, Utermann G, others (2009) Loss of dermatan-4-sulfotransferase 1 function results in adducted thumb-clubfoot syndrome. Am J Hum Genet 85:873–882
12. Esko JD, Kimata K, Lindahl U (2009) Proteoglycans and sulfated glycosaminoglycans. In: Varki A, Cummings RD, Esko JD, Freeze HH, Stanley P, Bertozzi CR, Hart GW, Etzler ME (eds) Essentials of glycobiology. Cold Spring Harbor, New York
13. Evers MR, Xia G, Kang HG, Schachner M, Baenziger JU (2001) Molecular cloning and characterization of a dermatan-specific N-acetylgalactosamine 4-O-sulfotransferase. J Biol Chem 276:36344–36353
14. Faiyaz-Ul-Haque M, Zaidi SH, Al-Ali M, Al-Mureikhi MS, Kennedy S, Al-Thani G, Tsui LC, Teebi AS (2004) A novel missense mutation in the galactosyltransferase-I (B4GALT7) gene in a family exhibiting facioskeletal anomalies and Ehlers-Danlos syndrome resembling the progeroid type. Am J Med Genet Part A 128A:39–45
15. Freeze HH (2006) Genetic defects in the human glycome. Nat Rev Genet 7:537–551
16. Hernandez A, Aguirre-Negrete MG, Gonzalez-Flores S, Reynoso-Luna MC, Fragoso R, Nazara Z, Tapia-Arizmendi G, Cantu JM (1986) Ehlers-Danlos features with progeroid facies and mild mental retardation. Further delineation of the syndrome. Clin Genet 30:456–461
17. Hernandez A, Aguirre-Negrete MG, Liparoli JC, Cantu JM (1981) Third case of a distinct variant of the Ehlers-Danlos Syndrome (EDS). Clin Genet 20:222–224
18. Hernandez A, Aguirre-Negrete MG, Ramirez-Soltero S, Gonzalez-Mendoza A, Martinez y Martinez R, Velazquez-Cabrera A, Cantu JM (1979) A distinct variant of the Ehlers-Danlos syndrome. Clin Genet 16:335–339
19. Jaeken J, Hennet T, Freeze HH, Matthijs G (2008) On the nomenclature of congenital disorders of glycosylation (CDG). J Inherit Metab Dis 31:669–672
20. Janecke AR, Baenziger JU, Müller T, Dündar M (2011) Loss of dermatan-4-sulfotransferase 1 (D4ST1/CHST14) function represents the first dermatan sulfate biosynthesis defect, "dermatan sulfate-deficient adducted thumb-club-foot syndrome". Hum Mutat 32:484–485
21. Janecke AR, Unsinn K, Kreczy A, Baldissera I, Gassner I, Neu N, Utermann G, Müller T (2001) Adducted thumb-club foot syndrome in sibs of a consanguineous Austrian family. J Med Genet 38:265–269
22. Kobe B, Deisenhofer J (1993) Crystal structure of porcine ribonuclease inhibitor, a protein with leucine-rich repeats. Nature 366:751–756
23. Kosho T, Miyake N, Hatamochi A, Takahashi J, Kato H, Miyahara T, Igawa Y, Yasui H, Ishida T, Ono K, others (2010) A new Ehlers-Danlos syndrome with craniofacial characteristics, multiple congenital contractures, progressive joint and skin laxity, and multisystem fragility-related manifestations. Am J Med Genet Part A 152A:1333–1346
24. Kosho T, Miyake N, Mizumoto S, Hatamochi A, Fukushima Y, Yamada S, Sugahara K, Matsumoto N (2011) A response to: loss of dermatan-4-sulfotransferase 1 (D4ST1/CHST14) function represents the first dermatan sulfate biosynthesis defect, "dermatan sulfate-deficient Adducted Thumb-Clubfoot Syndrome". Which name is appropriate, "Adducted Thumb-Clubfoot Syndrome" or "Ehlers-Danlos syndrome"? Hum Mutat 32:1507–1509
25. Kosho T, Takahashi J, Ohashi H, Nishimura G, Kato H, Fukushima Y (2005) Ehlers-Danlos syndrome type VIB with characteristic facies, decreased curvatures of the spinal column, and joint contractures in two unrelated girls. Am J Med Genet Part A 138A:282–287
26. Kresse H, Rosthoj S, Quentin E, Hollmann J, Glossl J, Okada S, Tonnesen T (1987) Glycosaminoglycan-free small proteoglycan core protein is secreted by fibroblasts from a patient with a syndrome resembling progeroid. Am J Hum Genet 41:436–453
27. Malfait F, Syx D, Vlummens P, Symoens S, Nampoothiri S, Hermanns-Le T, Van Laer L, De Paepe A (2010) Musculocontractural Ehlers-Danlos Syndrome (former EDS type VIB) and adducted thumb clubfoot syndrome (ATCS) represent a single clinical entity caused by mutations in the dermatan-4-sulfotransferase 1 encoding CHST14 gene. Hum Mutat 31:1233–1239
28. Malmström A (1984) Biosynthesis of dermatan sulfate. II. Substrate specificity of the C-5 uronosyl epimerase. J Biol Chem 259:161–165
29. Mao JR, Bristow J (2001) The Ehlers-Danlos syndrome: on beyond collagens. J Clin Invest 107:1063–1069
30. Mendoza-Londono R, Chitayat D, Kahr WH, Hinek A, Blaser S, Dupuis L, Goh E, Badilla-Porras R, Howard A, Mittaz L, others (2012) Extracellular matrix and platelet function in patients with musculo-

contractural Ehlers-Danlos syndrome caused by mutations in the CHST14 gene. Am J Med Genet Part A 158A:1344–1354
31. Miyake N, Kosho T, Mizumoto S, Furuichi T, Hatamochi A, Nagashima Y, Arai E, Takahashi K, Kawamura R, Wakui K, others (2010) Loss-of-function mutations of CHST14 in a new type of Ehlers-Danlos syndrome. Hum Mutat 31:966–974
32. Nakajima M, Mizumoto S, Miyake N, Kogawa R, Iida A, Ito H, Kitoh H, Hirayama A, Mitsubuchi H, Miyazaki O, others (2013) Mutations in B3GALT6, which encodes a glycosaminoglycan linker region enzyme, cause a spectrum of skeletal and connective tissue disorders. Am J Hum Genet 92:927–934
33. Okajima T, Fukumoto S, Furukawa K, Urano T (1999) Molecular basis for the progeroid variant of Ehlers-Danlos syndrome. Identification and characterization of two mutations in galactosyltransferase I gene. J Biol Chem 274:28841–28844
34. Okajima T, Yoshida K, Kondo T, Furukawa K (1999) Human homolog of Caenorhabditis elegans sqv-3 gene is galactosyltransferase I involved in the biosynthesis of the glycosaminoglycan-protein linkage region of proteoglycans. J Biol Chem 274:22915–22918
35. Scott JE (1988) Proteoglycan-fibrillar collagen interactions. Biochem J 252:313–323
36. Scott JE (1992) Morphometry of cupromeronic blue-stained proteoglycan molecules in animal corneas, versus that of purified proteoglycans stained in vitro, implies that tertiary structures contribute to corneal ultrastructure. J Anat 180(Pt 1):155–164
37. Scott JE (1995) Extracellular matrix, supramolecular organisation and shape. J Anat 187(Pt 2):259–269
38. Scott JE (1996) Proteodermatan and proteokeratan sulfate (decorin, lumican/fibromodulin) proteins are horseshoe shaped. Implications for their interactions with collagen. Biochemistry 35:8795–8799
39. Scott JE (2003) Elasticity in extracellular matrix 'shape modules' of tendon, cartilage, etc. A sliding proteoglycan-filament model. J Physiol 553:335–343
40. Seidler DG, Faiyaz-Ul-Haque M, Hansen U, Yip GW, Zaidi SH, Teebi AS, Kiesel L, Gotte M (2006) Defective glycosylation of decorin and biglycan, altered collagen structure, and abnormal phenotype of the skin fibroblasts of an Ehlers-Danlos syndrome patient carrying the novel Arg270Cys substitution in galactosyltransferase I (beta4GalT-7). J Mol Med (Berl) 84:583–594
41. Shimizu K, Okamoto N, Miyake N, Taira K, Sato Y, Matsuda K, Akimaru N, Ohashi H, Wakui K, Fukushima Y, others (2011) Delineation of dermatan 4-O-sulfotransferase 1 deficient Ehlers-Danlos syndrome: observation of two additional patients and comprehensive review of 20 reported patients. Am J Med Genet Part A 155A:1949–1958
42. Sisu E, Flangea C, Serb A, Zamfir AD (2011) Modern developments in mass spectrometry of chondroitin and dermatan sulfate glycosaminoglycans. Amino Acids 41:235–256
43. Sonoda T, Kouno K (2000) Two brothers with distal arthrogryposis, peculiar facial appearance, cleft palate, short stature, hydronephrosis, retentio testis, and normal intelligence: a new type of distal arthrogryposis? Am J Med Genet 91:280–285
44. Steinmann B, Royce PM, Superti-Furga A (2002) The Ehlers -Danlos syndrome. In: Royce PM and Steinmann B (eds) Connective tissue and its heritable disorders. (2nd edition) Wiley-Liss, Inc., New York
45. Sugahara K, Mikami T, Uyama T, Mizuguchi S, Nomura K, Kitagawa H (2003) Recent advances in the structural biology of chondroitin sulfate and dermatan sulfate. Curr Opin Struct Biol 13:612–620
46. Voermans NC, Kempers M, Lammens M, van Alfen N, Janssen MC, Bonnemann C, van Engelen BG, Hamel BC (2012) Myopathy in a 20-year-old female patient with D4ST-1 deficient Ehlers-Danlos syndrome due to a homozygous CHST14 mutation. Am J Med Genet Part A 158A:850–855
47. Weber IT, Harrison RW, Iozzo RV (1996) Model structure of decorin and implications for collagen fibrillogenesis. J Biol Chem 271:31767–31770
48. Winters KA, Jiang Z, Xu W, Li S, Ammous Z, Jayakar P, Wierenga KJ (2012) Re-assigned diagnosis of D4ST1-deficient Ehlers-Danlos syndrome (adducted thumb-clubfoot syndrome) after initial diagnosis of Marden-Walker syndrome. Am J Med Genet A 158A:2935–2940
49. Yasui H, Adachi Y, Minami T, Ishida T, Kato Y, Imai K (2003) Combination therapy of DDAVP and conjugated estrogens for a recurrent large subcutaneous hematoma in Ehlers-Danlos syndrome. Am J Hematol 72:71–72

Neurogenetics (2014) 15:85–92
DOI 10.1007/s10048-013-0384-7

ORIGINAL ARTICLE

PIGN mutations cause congenital anomalies, developmental delay, hypotonia, epilepsy, and progressive cerebellar atrophy

Chihiro Ohba · Nobuhiko Okamoto · Yoshiko Murakami · Yasuhiro Suzuki · Yoshinori Tsurusaki · Mitsuko Nakashima · Noriko Miyake · Fumiaki Tanaka · Taroh Kinoshita · Naomichi Matsumoto · Hirotomo Saitsu

Received: 2 November 2013 / Accepted: 10 November 2013 / Published online: 20 November 2013

Abstract Defects of the human glycosylphosphatidylinositol (GPI) anchor biosynthetic pathway show a broad range of clinical phenotypes. A homozygous mutation in *PIGN*, a member of genes involved in the GPI anchor-synthesis pathway, was previously reported to cause dysmorphic features, multiple congenital anomalies, severe neurological impairment, and seizure in a consanguineous family. Here, we report two affected siblings with compound heterozygous *PIGN* mutations [c.808T >C (p.Ser270Pro) and c.963G >A] showing congenital anomalies, developmental delay, hypotonia, epilepsy, and progressive cerebellar atrophy. The c.808C >T mutation altered an evolutionarily conserved amino acid residue (Ser270), while reverse transcription-PCR and sequencing demonstrated that c.963G >A led to aberrant splicing, in which two mutant transcripts with premature stop codons (p.Ala322Valfs*24 and p.Glu308Glyfs*2) were generated. Expression of GPI-anchored proteins such as CD16 and CD24 on granulocytes from affected siblings was

Chihiro Ohba, Nobuhiko Okamoto, and Yoshiko Murakami contributed equally

Electronic supplementary material The online version of this article (doi:10.1007/s10048-013-0384-7) contains supplementary material, which is available to authorized users.

C. Ohba · Y. Tsurusaki · M. Nakashima · N. Miyake · N. Matsumoto · H. Saitsu (✉)
Department of Human Genetics, Graduate School of Medicine, Yokohama City University, 3-9 Fukuura, Kanazawa-ku, Yokohama 236-0004, Japan
e-mail: hsaitsu@yokohama-cu.ac.jp

C. Ohba
e-mail: t116017g@yokohama-cu.ac.jp

Y. Tsurusaki
e-mail: tsurusak@yokohama-cu.ac.jp

M. Nakashima
e-mail: mnakashi@yokohama-cu.ac.jp

N. Miyake
e-mail: nmiyake@yokohama-cu.ac.jp

N. Matsumoto
e-mail: naomat@yokohama-cu.ac.jp

C. Ohba · F. Tanaka
Department of Clinical Neurology and Stroke Medicine, Yokohama City University, Yokohama 236-0004, Japan

F. Tanaka
e-mail: ftanaka@yokohama-cu.ac.jp

N. Okamoto
Department of Medical Genetics, Osaka Medical Center and Research Institute for Maternal and Child Health, Izumi 594-1101, Japan
e-mail: okamoto@osaka.email.ne.jp

Y. Murakami · T. Kinoshita
Department of Immunoregulation, Research Institute for Microbial Diseases, Osaka University, Osaka 565-0871, Japan

Y. Murakami
e-mail: yoshiko@biken.osaka-u.ac.jp

T. Kinoshita
e-mail: tkinoshi@biken.osaka-u.ac.jp

Y. Murakami · T. Kinoshita
World Premier International Immunology Frontier Research Center, Osaka University, Osaka 565-0871, Japan

Y. Suzuki
Department of Pediatric Neurology, Osaka Medical Center and Research Institute for Maternal and Child Health, Osaka, Japan
e-mail: yasuzuki@mch.pref.osaka.jp

significantly decreased, and expression of the GPI-anchored protein CD59 in *PIGN*-knockout human embryonic kidney 293 cells was partially or hardly restored by transient expression of p.Ser270Pro and p.Glu308Glyfs*2 mutants, respectively, suggesting severe and complete loss of PIGN activity. Our findings confirm that developmental delay, hypotonia, and epilepsy combined with congenital anomalies are common phenotypes of *PIGN* mutations and add progressive cerebellar atrophy to this clinical spectrum.

Keywords Cerebellar atrophy · Compound heterozygous mutation · Glycosylphosphatidylinositol anchor · *PIGN*

Introduction

Defects of the biosynthetic pathway of the glycosylphosphatidylinositol (GPI) anchor cause broad clinical phenotypes [1]. The products of more than 20 genes in the phosphatidylinositol glycan (PIG) family are involved in GPI biosynthesis, whereas post-GPI-attachment to proteins (PGAP) gene products play a role in the structural remodeling of GPI glycan and lipid portions [2]. Mutations in eight genes involved in GPI biosynthesis and remodeling (*PIGA*, *PIGM*, *PIGN*, *PIGV*, *PIGL*, *PIGO*, *PIGT*, and *PGAP2*) have been identified in individuals with neurological abnormalities [1, 3–5], of which *PIGN* controls the addition of phosphoethanolamine to the first mannose in GPI [6]. To date, only one homozygous *PIGN* mutation has been reported to cause dysmorphic features, multiple congenital anomalies, severe neurological impairment, and seizures in a consanguineous family [7]. Here, we report a family with two affected siblings, possessing compound heterozygous *PIGN* mutations. Detailed clinical information and molecular and functional analyses are presented.

Patients and methods

Patients

We analyzed two affected siblings and their parents. Experimental protocols were approved by the Institutional Review Board of Yokohama City University School of Medicine. Clinical information and peripheral blood samples were acquired from the family members after obtaining written informed consent. Patient clinical features are summarized in Table 1. They showed dysmorphic facial features, developmental delay, intellectual disability, hypotonia, vertical nystagmus, and epilepsy.

Patient 1

This 9-year-old girl was born to nonconsanguineous healthy parents as a second child after 39 weeks of gestation (Fig. 1a). Her birth weight was 3,390 g [+1.40 standard deviation (SD)], body length of 49 cm (−0.03 SD), and head circumference of 35 cm (+1.35 SD). At 1 month of age, she showed vertical nystagmus without eye pursuit. She was hypotonic, and severe developmental delay was evident from early infancy. She was unable to control her head or utter words at 9 years of age. Abdominal echogram revealed bilateral vesicoureteral reflux as a cause of repeated urinary tract infections. Complex partial seizures developed at 8 months of age and were controlled by antiepileptic drugs. Tube feeding by gastrostomy was necessary for poor appetite at the age of 2 years.

Several dysmorphic features (prominent occiput, bitemporal narrowing, epicanthal folds, open mouth, tented upper lip, high arched palate, micrognathia, and deep plantar groove) were noted (Fig. 1b), but hypoplasia was absent from fingers and fingernails. Initial brain magnetic resonance imaging (MRI) at 6 months of age was normal, but cerebellar atrophy was observed at 2 and 6 years of age (Fig. 1c–f).

At present, her height is 122 cm (+1.1 SD), weight of 18.4 kg (−1.2 SD), and head circumference of 51.4 cm (−0.3 SD). Generalized muscle weakness and nystagmus were neurologically recognized. Laboratory examination showed a normal profile, including blood cell count and blood smear, renal and liver function, total bilirubin, uric acid, albumin, serum electrolytes, lactate, pyruvate, ammonia, amino acids, blood gasses, thyroid function, and cerebrospinal fluid study. Her serum alkaline phosphatase (ALP) activity has been normal for her age since infancy. Metabolic disorder screening including organic acid analysis, lysosomal enzymes, and mass spectrometry of transferrin was normal. G-banded analysis showed a normal karyotype (46, XX).

Patient 2

This 2-year-old boy was born after 37 weeks of gestation as a younger brother to patient 1 (Fig. 1a). His birth weight was 3,252 g (+1.3 SD), body length of 50 cm (+1.2 SD), and head circumference of 35 cm (+1.6 SD). He also showed vertical nystagmus at 1 month of age. Complex partial seizures developed at 5 months of age. He was hypotonic, and his developmental milestones were severely delayed with no head control at 1 year and 10 months of age. At present, his height is 92.3 cm (+2.5 SD), weight of 10.9 kg (−0.6 SD), and head circumference of 48.8 cm (+0.4 SD). He showed similar dysmorphic features to patient 1. Brain MRI at 2 months of age revealed no significant abnormalities.

Table 1 Clinical features of patients with *PIGN* mutations

Patient	1	2	Reported by Maydan et al. [7]							
			V-1	V-2	V-4	V-5	V-8	V-9	V-10	Total
Age (years)	9	2	N.D.	Diseased at 14	Diseased at 1	Diseased at 5	Diseased at 3	Diseased at 17	Diseased at 39	
Sex	Female	Male	Male	Male	Male	Female	Female	Female	Male	
Size at birth (percentile)										
Weight (g)	3,390 (90–97)	3,252 (90–97)	3,566 (95)	4,065 (97)	3,850 (95)	3,410 (40)	4,250 (99)	4,300 (98)	4,800 (>99)	
Head circumference (cm)	35 (90)	35 (90–97)	37 (>97)	37 (97)	35.5 (75)	34.5 (10)	N.D.	N.D.	N.D.	
Abnormalities										
Facial features	+	+	+	+	+	+	+	+	+	9/9
Fingers/foot	+	+	+	+	+	-	–	+	+	6/9
Heart	–	–	+	+	+	+	–	+	–	5/9
Urinary tract	+	–	+	+	+	–	–	–	–	4/9
Gastrointestinal tract	GER	–	GER	GER	Anal stenosis	Imperforate anus, ano-vestibular fistula, GER	–	Feeding and swallowing difficulties	Feeding and swallowing difficulties	7/9
Neurological features										
Developmental delay	+	+	+	+	+	+	+	+	+	9/9
Hypotonia	+	+	+	+	+	+	+	+	+	9/9
Nystagmus	+	+	+	+	–	+	–	+	+	7/9
Tremor	+	+	+	+	+	+	+	–	–	7/9
Seizure	+	+	+	–	+	+	+	+	+	8/9
Brain CT	Normal	Normal	Normal	N.D.	Normal	Multiple small subdural hematomas	N.D.	N.D.	N.D.	1/5
Brain MRI				N.D.	N.D.		N.D.	N.D.	N.D.	
Delayed myelination	+	–	–			+				2/4
Thin corpus callosum	–	–	–			+				1/4
Cerebellar atrophy	+	–	Minimal loss of vermis parenchyma			–				1/4
Enlargement of the ventricle	+	–	–			+ (Mild)				2/4

GER Gastroesophageal reflux, *N.D.* not determined

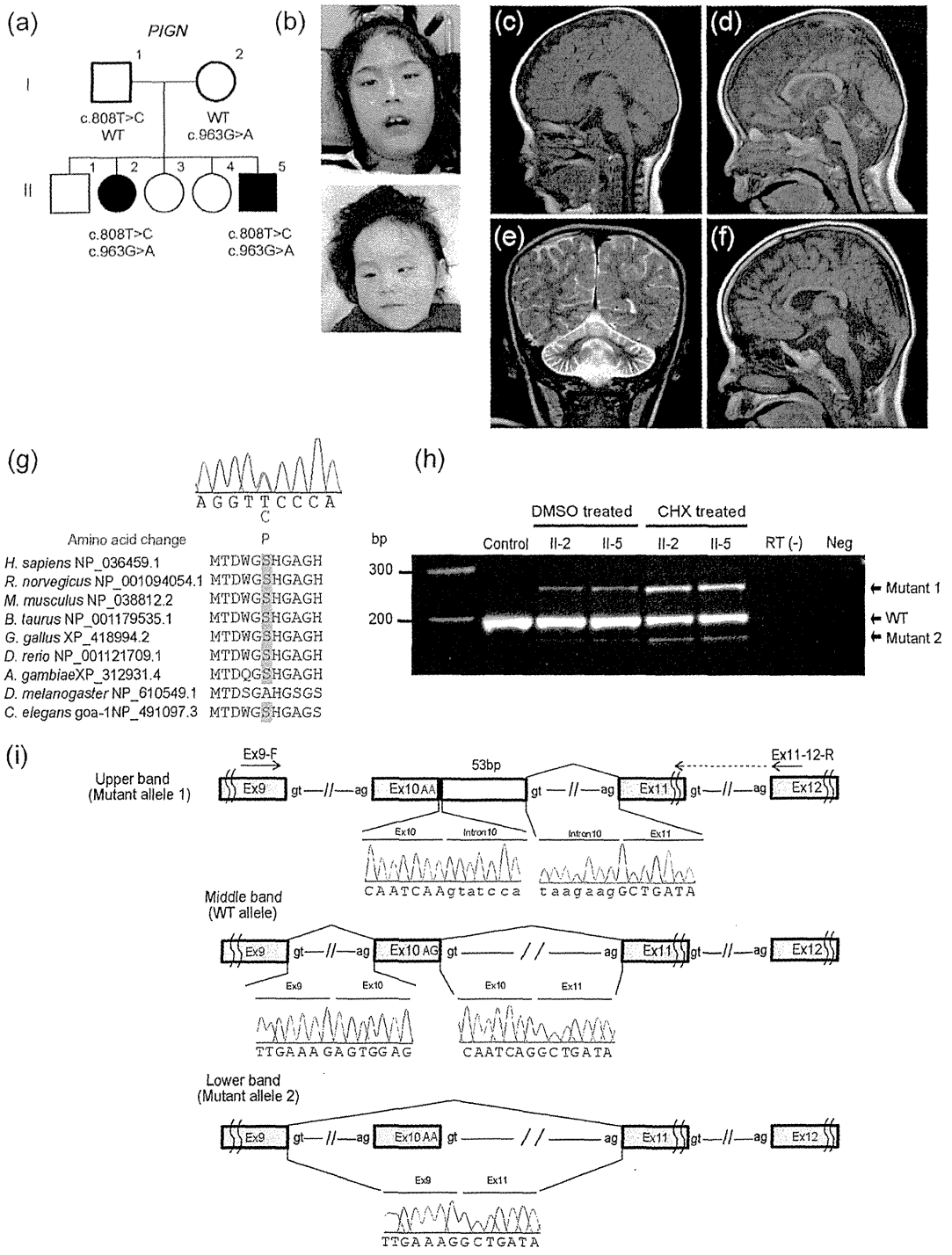

Whole exome sequencing (WES)

Genomic DNA was isolated from peripheral blood leukocytes, captured using the SureSelect Human All Exon v4 Kit (51 Mb; Agilent Technologies, Santa Clara, CA), and sequenced on an Illumina HiSeq2000 (Illumina, San Diego, CA) with 101 bp paired-end reads. Data processing, variant calling, and variant annotation were performed as previously described [8].

◀ **Fig. 1** **a** Familial pedigree and mutations. **b** Photographs of the faces of patient 1 (*upper*) and patient 2 (*lower*). Frontal narrow temporal, frontal bossing, hypertelorism, epicanthal folds, down-slanting palpebral fissures, high nasal bridge, bilateral low set ears, thin philtrum, downturned mouth, and microretrognathia are noted in both patients. **c**, **d**, **f** T1-weighted midline sagittal images and **e** T2-weighted coronal images of patient 1 (**c** at 6 months, **d** and **e** at 2 years, and **i** at 6 years). Progressive vermis atrophy (**c**, **d**, **f**) and hemispheres atrophy (**e**) were observed. **g** Sequence chromatography showing heterozyogous c.808C >T mutation, which alters an evolutionarily conserved amino acid. Homologous sequences were aligned using CLUSTALW. **h** RT-PCR analysis using cDNA of LCLs derived from two patients (II-2 and II-5) and a control. **i** Schematic representation of wild-type (WT) and mutant transcripts and primers used for the analysis. Primer of ex11-12-R spans exons 11 and 12. A single band (200 bp), corresponding to the WT allele, was amplified using control cDNA. Upper and lower bands were detected from patient cDNA. The upper band (253 bp) has a 53-bp insertion of intron 10 sequences, leading to a frameshift mutation. The lower band has a 41-bp deletion of the entire exon 10, also leading to a frameshift mutation

Reverse transcriptase-PCR

Lymphoblastoid cell lines (LCLs) were established from the two patients. RT-PCR using total RNA extracted from LCLs was performed as previously described [9].

Briefly, total RNA was extracted using the RNeasy Plus Mini kit (Qiagen, Tokyo, Japan) from LCLs with or without incubation in 30 μM cycloheximide (CHX; Sigma, Tokyo, Japan) for 4 h. Four micrograms of total RNA was subjected to reverse transcription, and 2 μl cDNA was used for PCR. Primer sequences were ex9-F (5′-TCCTTTAGTCACTTGG GGAGCTGGA-3′) and ex11-12-R (5′-AATCCACAGGAA GGATTCCCACTGA-3′) (Supplementary Table 1). PCR products were electrophoresed on a 10 % polyacrylamide gel and sequenced. PCR bands were purified by the E.Z.N.A. poly-Gel DNA Extraction kit (Omega Bio-Tek, Norcross, GA).

Fluorescence-activated cell sorting (FACS) analysis

Surface expression of GPI-anchored proteins (GPI-APs) was determined by staining cells with Alexa 488-conjugated inactivated aerolysin [fluorescently-labeled inactive toxin aerolysin (FLAER); Protox Biotech, Victoria, BC, Canada] and appropriate primary antibodies: mouse anti-decay accelerating factor (DAF; IA10), −CD16 (3G8), −CD24 (ML5), −CD59 (5H8), and −CD48 (BJ40) followed by a PE-conjugated anti-mouse IgG antibody (3G8, ML5, BJ40, and secondary antibodies; BD Biosciences, Franklin Lakes, NJ). Cells were analyzed by flow cytometry (Cant II; BD Biosciences) with Flowjo software (v9.5.3, Tommy Digital, Tokyo, Japan).

Functional analysis in HEK293 cells

PIGN-knockout cells were generated from HEK293 cells using the CRISPR/Cas System [10]. We obtained the human codon-optimized *Streptococcus pyogenes* Cas9 and chimeric guide RNA expression plasmid pX330 from Addgene (Cambridge, MA). The seed sequence for the SpCas9 target site in *PIGN* exon 4 (CCA-GGTCATGTAGCTCTGATAGC) was selected and a pair of annealed oligos designed according to this sequence and cloned into the *Bbs* I sites of pX330. HEK293 cells were transfected with pX330 containing the target site using Lipofectamine 2000 (Invitrogen, Carlsbad, CA). Cells were stained with anti-CD59 antibody 14 days after transfection, and *PIGN*-knockout clones were obtained by limiting dilution.

PIGN-knockout HEK293 cells (clone PIGNKO2-12) were transiently transfected with a wild-type or mutant (S290P or exon 10 skipping) *PIGN* cDNA cloned into the SRα promoter-driven expression vector pME HA-PIGN. Restoration of the surface expression of CD59, DAF, and GPI-APs was assessed 2 days later by flow cytometry.

Results

WES detected 288 and 292 rare protein-altering and splice-site variants in patients 1 and 2, respectively. We filtered out common single nucleotide polymorphisms (SNPs) that met the following two criteria: variants showing minor allele frequencies ≥1 % in dbSNP 135 and variants found in more than two of our in-house 406 control exomes (Supplementary Table 2). All genes were surveyed for compound heterozygous or homozygous mutations consistent with an autosomal recessive trait, and only *PIGN* (GenBank accession number NM_176787.4) met this criterion, possessing compound heterozygous mutations in two patients. The missense mutation c.808T >C (p.Ser270Pro) was inherited from the patients' father, while c.963G >A is a synonymous mutation inherited from their mother but located at the last base of exon 10 (Fig. 1i). Neither of the two mutations was present in the 6,500 exomes sequenced by the National Heart, Lung, and Blood Institute exome project. In our 406 in-house control exomes, c.808T >C was absent, but c.963G >A was found in one, as a heterozygous mutation. c.808T >C occurred at evolutionary conserved amino acids (Fig. 1g) and was predicted to be pathogenic using online software (Supplementary Table 3). To examine the actual effects of c.963G >A on splicing, RT-PCR was performed (Fig. 1h, i) and a single band (200 bp) corresponding to the wild-type *PIGN* allele was amplified from control LCL cDNA template (Fig. 1h). By contrast, two aberrant faint bands were detected in addition to a wild-type band from patient cDNA (Fig. 1h). Sequencing of the upper aberrant band indicated a 53-bp insertion of intron 10 sequences that had

used a cryptic splice donor site within intron 10, producing a premature stop codon (p.Ala322Valfs*24). Sequencing of the lower band demonstrated the deletion of exon 10 from wild-type *PIGN* mRNA, also producing a premature stop codon (p.Glu308Glyfs*2). Therefore, these two mutant transcripts are likely to be degraded by nonsense-mediated mRNA decay (NMD). In fact, CHX treatment, which inhibits NMD, increased the intensity of the aberrant bands, suggesting that NMD was indeed involved.

To examine the functional impairment of *PIGN* caused by compound heterozygous mutations, the surface expression of various GPI-APs was analyzed by flow cytometry. CD16 and CD24 expression on blood granulocytes was decreased to 26–54 % of normal levels in both patients (Fig. 2a). No abnormal GPI-APs expression was observed on LCLs from either patient (Supplementary Fig. 1).

Transient expression of p.Ser270Pro and exon 10 skipping (p.Glu308Glyfs*2) mutants in *PIGN*-knockout HEK293 cells, in which expression of GPI-APs CD59 was decreased, was confirmed by immunoblotting. Expression of the exon 10 skipping mutant was decreased compared with that of wild-type and p.Ser270Pro mutant (Supplementary Fig. 2). CD59 expression was only partially or hardly restored by the transient expression of p.Ser270Pro and exon 10 skipping mutants, respectively, suggesting severe or complete loss of PIGN activity (Fig. 2b).

Discussion

Herein, we report a second family with *PIGN* mutations that showed clinical features common to a previous affected family, including congenital anomalies, developmental delay, hypotonia, and epilepsy [7]. In addition, nystagmus was an early symptom of patients in this study and was also observed in five of seven patients previously [7]. Of note, progressive cerebellar atrophy was observed in the current patient 1, and this appears to be a novel phenotype associated with *PIGN*

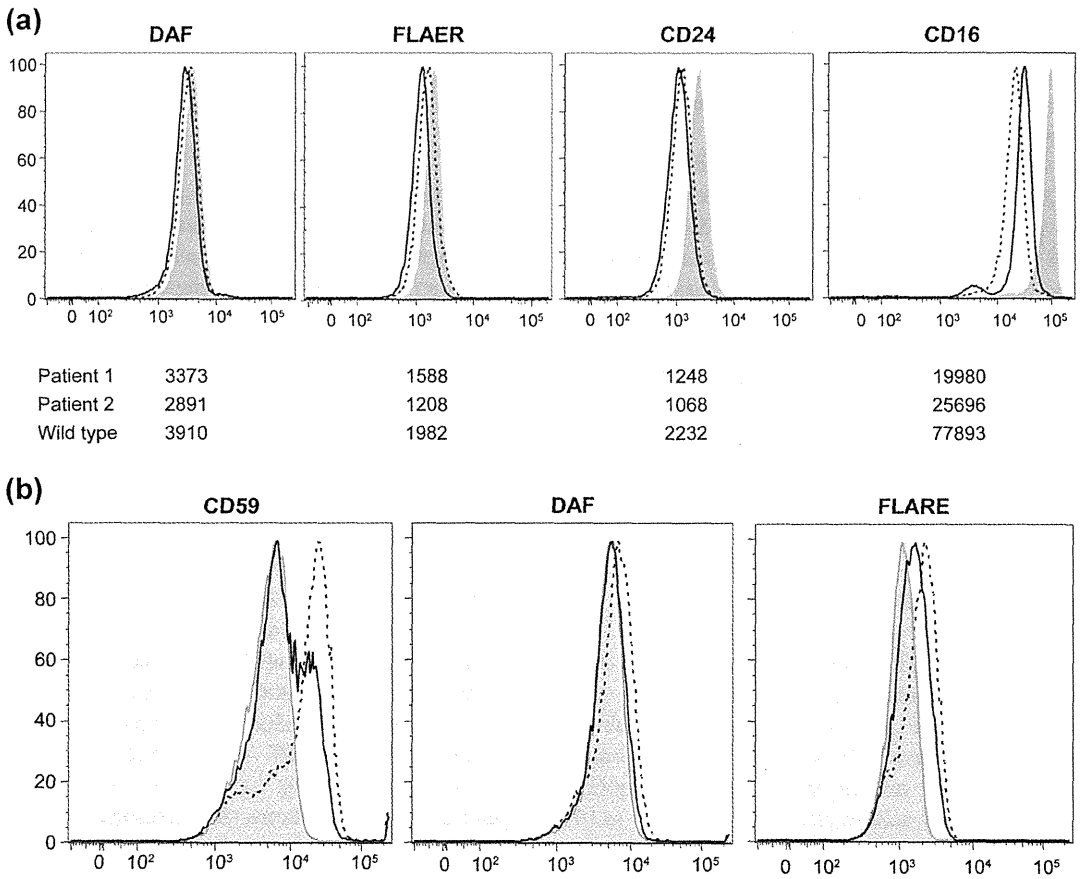

Fig. 2 **a** Surface expression of various GPI-APs on patient granulocytes (patient 1: *dotted lines*, patient 2: *solid lines*), a normal control (*dark shadow*) and an isotype control (*light shadows*). Numbers represent mean fluorescent intensities. Expression of DAF and FLAER in both patients did not significantly change compared with the control. However, CD16 and CD24 expression decreased to 26–54 % of normal levels. **b** *PIGN*-knockout HEK293 cells were transiently transfected with wild type (*dotted lines*) or mutants (exon 10 skipping: *gray line*, p.Ser270Pro: *black line*) of pME HA-PIGN vectors. Empty vector: *dark shadow*, isotype control: *light shadow*. Expression of CD59 was only partially or hardly restored by p.Ser270Pro and exon 10-skipping vectors, respectively

mutations as two patients examined by MRI showed no cerebellar atrophy but only minimal loss of vermis parenchyma in one patient (patient V-1) in the previous report [7].

PIGN is involved in the addition of phosphoethanolamine to the first mannose in GPI [6]. In *Pign*-knockout mouse F9 embryonal carcinoma cells, the first mannose in GPI precursors is not modified by phosphoethanolamine. Nevertheless, further biosynthetic steps continue and the cell surface expression of GPI-anchored proteins is only partially affected [6], suggesting that this modification may not be essential for GPI-anchored protein biosynthesis [6]. By contrast, the *gonzo* mouse line, which harbors the splice donor site mutation in *Pign*, showed abnormal forebrain development resembling holoprosencephaly [11], and patients with *PIGN* mutations show severe phenotypes such as multiple congenital anomalies, neurological impairment, and even lethality [7]; this indicates that particular defects of *PIGN*/*Pign* cause abnormal development both in mice and humans. Although the overall amount of GPI-anchored proteins might not be significantly affected by *PIGN* defects, as revealed by the minimal decrease in DAF and FLAER expression on patient granulocytes in the present study, changes to a subset of GPI-anchored proteins such as CD16 and CD24 can be sufficient to cause severe neurological phenotypes. Additionally or alternatively, GPI-APs expressed on PIGN-defective cells lack the phosphoethanolamine-side branch, and this abnormal structure of the glycan part of the anchor might affect functions of GPI-APs. Functional analysis using neuronal cells may provide novel insights into the pathogenesis of neurological phenotypes caused by *PIGN* mutations.

Seven genes (*PIGA*, *PIGM*, *PIGN*, *PIGV*, *PIGL*, *PIGO*, and *PGAP2*) have been identified as being mutated in patients with neurological abnormalities. Mutations in three of these (*PIGV*, *PIGO*, and *PGAP2*) cause hyperphosphatasia [3, 12–14], suggesting that ALP is a useful marker for suspected GPI anchor-synthesis pathway deficiencies. However, mutations of the other four genes (*PIGA*, *PIGM*, *PIGN*, and *PIGL*) did not cause hyperphosphatasia [7, 14, 15], so clinical diagnosis might be difficult in the absence of specific biomarkers. Even in clinically unsuspected patients, WES may identify mutations in genes involved in the GPI anchor-synthesis pathway. Current advances in next generation sequencing should find more comprehensive answers for unsolved GPI anchor-related diseases.

Acknowledgments We would like to thank patients and their parents for their participation in this study. We also thank Nobuko Watanabe and Kana Miyanagi for technical assistance. This work was supported by the Ministry of Health, Labour, and Welfare of Japan; a Grant-in-Aid for Scientific Research (A), (B), and (C) from the Japan Society for the Promotion of Science (A: 24249019, B: 25293085 25293235, C: 23590363); the Takeda Science Foundation; the Japan Science and Technology Agency; the Strategic Research Program for Brain Sciences (11105137); and a Grant-in-Aid for Scientific Research on Innovative Areas (Transcription Cycle, Exploring molecular basis for brain diseases based on personal genomics) from the Ministry of Education, Culture, Sports, Science, and Technology of Japan (12024421, 25129705).

References

1. Freeze HH, Eklund EA, Ng BG, Patterson MC (2012) Neurology of inherited glycosylation disorders. Lancet Neurol 11(5):453–466. doi:10.1016/s1474-4422(12)70040-6
2. Maeda Y, Kinoshita T (2011) Structural remodeling, trafficking and functions of glycosylphosphatidylinositol-anchored proteins. Prog Lipid Res 50(4):411–424. doi:10.1016/j.plipres.2011.05.002
3. Hansen L, Tawamie H, Murakami Y, Mang Y, ur Rehman S, Buchert R, Schaffer S, Muhammad S, Bak M, Nothen MM, Bennett EP, Maeda Y, Aigner M, Reis A, Kinoshita T, Tommerup N, Baig SM, Abou Jamra R (2013) Hypomorphic mutations in *PGAP2*, encoding a GPI-anchor-remodeling protein, cause autosomal-recessive intellectual disability. Am J Hum Genet 92(4):575–583. doi:10.1016/j.ajhg.2013.03.008
4. Krawitz PM, Murakami Y, Riess A, Hietala M, Kruger U, Zhu N, Kinoshita T, Mundlos S, Hecht J, Robinson PN, Horn D (2013) *PGAP2* mutations, affecting the GPI-anchor-synthesis pathway, cause hyperphosphatasia with mental retardation syndrome. Am J Hum Genet 92(4):584–589. doi:10.1016/j.ajhg.2013.03.011
5. Kvarnung M, Nilsson D, Lindstrand A, Korenke GC, Chiang SC, Blennow E, Bergmann M, Stodberg T, Makitie O, Anderlid BM, Bryceson YT, Nordenskjold M, Nordgren A (2013) A novel intellectual disability syndrome caused by GPI anchor deficiency due to homozygous mutations in *PIGT*. J Med Genet 50(8):521–528. doi:10.1136/jmedgenet-2013-101654
6. Hong Y, Maeda Y, Watanabe R, Ohishi K, Mishkind M, Riezman H, Kinoshita T (1999) Pig-n, a mammalian homologue of yeast Mcd4p, is involved in transferring phosphoethanolamine to the first mannose of the glycosylphosphatidylinositol. J Biol Chem 274(49):35099–35106
7. Maydan G, Noyman I, Har-Zahav A, Neriah ZB, Pasmanik-Chor M, Yeheskel A, Albin-Kaplanski A, Maya I, Magal N, Birk E, Simon AJ, Halevy A, Rechavi G, Shohat M, Straussberg R, Basel-Vanagaite L (2011) Multiple congenital anomalies-hypotonia-seizures syndrome is caused by a mutation in *PIGN*. J Med Genet 48(6):383–389. doi:10.1136/jmg.2010.087114
8. Saitsu H, Nishimura T, Muramatsu K, Kodera H, Kumada S, Sugai K, Kasai-Yoshida E, Sawaura N, Nishida H, Hoshino A, Ryujin F, Yoshioka S, Nishiyama K, Kondo Y, Tsurusaki Y, Nakashima M, Miyake N, Arakawa H, Kato M, Mizushima N, Matsumoto N (2013) *De novo* mutations in the autophagy gene *WDR45* cause static encephalopathy of childhood with neurodegeneration in adulthood. Nat Genet. doi:10.1038/ng.2562
9. Saitsu H, Kato M, Okada I, Orii KE, Higuchi T, Hoshino H, Kubota M, Arai H, Tagawa T, Kimura S, Sudo A, Miyama S, Takami Y, Watanabe T, Nishimura A, Nishiyama K, Miyake N, Wada T, Osaka H, Kondo N, Hayasaka K, Matsumoto N (2010) *STXBP1* mutations in early infantile epileptic encephalopathy with suppression-burst pattern. Epilepsia 51(12):2397–2405. doi:10.1111/j.1528-1167.2010.02728.x
10. Cong L, Ran FA, Cox D, Lin S, Barretto R, Habib N, Hsu PD, Wu X, Jiang W, Marraffini LA, Zhang F (2013) Multiplex genome engineering using CRISPR/Cas systems. Science 339(6121):819–823. doi:10.1126/science.1231143
11. McKean DM, Niswander L (2012) Defects in GPI biosynthesis perturb Cripto signaling during forebrain development in two new mouse models of holoprosencephaly. Biology open 1(9):874–883. doi:10.1242/bio.20121982
12. Freeze HH (2013) Understanding human glycosylation disorders: biochemistry leads the charge. J Biol Chem 288(10):6936–6945. doi:10.1074/jbc.R112.429274